Monolayer to Multilayer Nanostructural Evolution in N type Oligothiphenes: Implications for OFET Performance

Geetha R Dholakia[1a], Antonio Facchetti[2b], and Tobin J Marks[2c]

1. NASA Ames Research Center, Moffett Field CA 94035
2. Department of Chemistry, Northwestern University, Evanston, IL 60208.

Abstract

We present the evolution in the growth morphology and molecular orientation of an n-type fluorocarbon-substituted quaterthiophene DFH-4T by scanning tunneling microscopy, as the film thickness is increased from one monolayer to many multilayers. In parallel we measured the performance of top vs bottom contact DFH-4T organic field effect transistors and show a three orders of magnitude difference in performance. By correlating the observed nanostructure with the device properties, we show that the superior performance of top contact devices is due to the better molecular orientation and alignment in multilayer films with respect to the contacts.

Keywords: monolayer, thiophenes, organic FETs, scanning tunneling microscopy.

Introduction

Organic electronics holds tremendous potential for applications requiring structural flexibility and large area coverage and has the added advantage of low fabrication costs. The range of potential applications include low end data storage devices, identification tags and display devices [1]. In the last few years, the mobilities of organic field effect transistors (OFETs) have increased enough to be of use in technological applications. Some of the critical molecular parameters that influence mobilities in OFET devices include molecular orientation and interchain stacking. Morphological features such as grain boundaries and defects at the film-substrate and film-source-drain contact interfaces act as scattering centers and charge traps, degrading the performance and lead to inefficient charge transport and low mobility values as compared to conventional CMOS devices.. Typical organic film thickness in OFETs range from 50-100 nm and involve the stacking of several oligomeric layers, requiring the organic semiconductor to be deposited on a variety of substrate materials and metallic source-drain contacts. Understanding the mechanism of organic film growth on dielectric and metallic interfaces, its orientational relationship within the multilayers and with the substrates, as well as optimizing the growth parameters is critical to achieving OFET devices with high mobilities [2]. This paper discusses the evolution in the nanostructure of an n-type organic semiconductor on gold substrates, as the thickness increases from one monolayer to many multilayers. We seek to understand how these morphological changes impact the OFET device performance. In parallel, we also analyze charge transport and contact resistance of top-contact and bottom-contact OFETs and relate this to the film morphology.

Experimental Details

The n-type organic semiconductor chosen for this study is a fluorocarbon-substituted quaterthiophene (α,ω-diperfluorohexyl-4T), DFH-4T. The DFH-4T crystal structure illustrating molecular orientation and packing is shown in Figure 1. Top-contact OFETs fabricated from this oligomer exhibit excellent n-type transport, however, as for many n-type fluorocarbon-substituted semiconductors, it exhibits poor charge transport in bottom-contact devices. The synthesis of DFH-4T is described elsewhere [3]. The motivation here is to understand how morphological features of organic semiconducting films on metal contacts evolve on the nanoscale as film thickness increases from one monolayer to many multilayers and to thicknesses of typical OFETs. We correlate the film's nanostructural features such as orientation and molecular alignment on the metal contacts, the presence of structural defects, grain boundaries and other scattering centers with OFET charge transport characteristics.

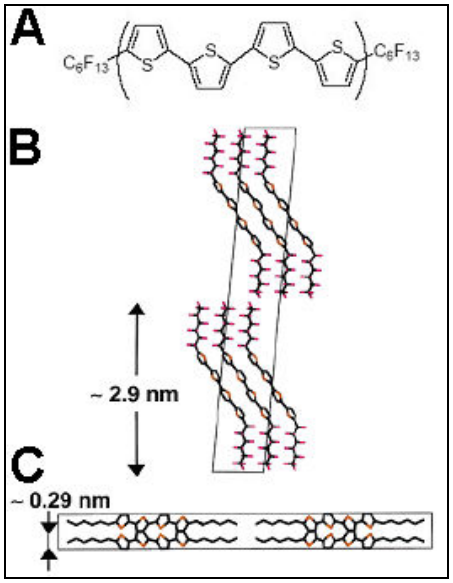

Fig. 1 DFH-4T structure and orientation.

Nanostructural evolution in four DFH-4T films of thicknesses 3, 5, 10 and 12 nm, obtained by evaporating DFH-4T (0.2 – 0.4 $Å s^{-1}$, $p \approx 10^{-6}$ Torr, 50 nm) onto flame annealed Au(111) substrates is studied by scanning tunneling microscopy (Oxford-STM). All the measurements were performed in vacuum (~ 10^{-6} Torr) using cut Pt\Ir tips. Topographic images were obtained in the constant current mode with a bias of 1.0 V and a typical set point tunnel current of 10-100 pA, which ensures a large tunnel junction impedance of 100-10 GΩ and thus avoids destructive tip–surface interactions. The density of states (DOS) of DFH-4T\Au(111) was probed by scanning tunneling spectroscopy (STS), using a typical set point bias of 0.50 V and a set point current of 50 pA, corresponding to a junction impedance of 10 GΩ. Each I-V spectra is recorded as an average of 7 individual curves. OFETs were fabricated by evaporating DFH-4T onto p^+-Si/SiO_2 (300 nm oxide) substrates at 70 °C. For bottom- and top-contact devices, Au source and drain electrodes (50 nm) were vapor-deposited through a shadow mask before and after DFH-4T deposition, respectively. OFET measurements were carried out in air with a Signaton probe station using a Keithley 6430 subfemtoammeter and a Keithley 2400 source meter interfaced by Labview.

Results and Discussion

Figures 2 and 3 show the morphological features of the DFH-4T films on Au(111), presented in comparable scan ranges in the order of increasing film thickness, beginning with the 3 nm films. Flame-annealing of the gold surface ensures an atomically smooth Au(111) substrate. Single-crystal X-ray diffraction data on DFH-4T provides a molecular length of 3.325 nm and XRD of DFH-4T thin films on Si/SiO_2 reveals that the films have a *d* spacing of 2.93 nm, with the long molecular axes of the oligothiophene molecules aligned along the surface normal (see Fig. 1). Thus, a monolayer of the film should approximately be 3 nm in thickness and the films studied here by the STM span a range from one monolayer through four multilayers.

Figures 2A,B show the nanostructure of the 3 nm thick DFH-4T film in the 2 μm and 1 μm scan ranges respectively. The images show the organic molecule completely covering the gold surface and the film otherwise appearing featureless except for a number pits and defects (15-50 nm dia.) observed as dark depressions. The images also show the underlying Au(111) substrate terraces intersecting at 120° angles. It is important to note that no grains or grain boundaries are observed in the 3 nm DFH-4T film. Figures 2C,D are images from different regions of a 5 nm-thick film.

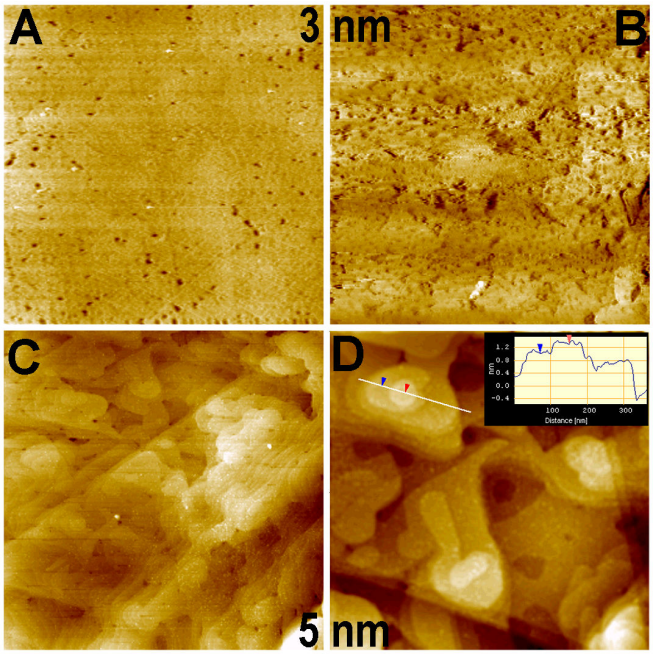

Fig. 2 Morphology of 3 nm and 5 nm thick films in 2 μm (right) and 1 μm scans (left). Inset shows a profile across a terrace with a step height of 0.29 nm.

The change in the nanostructure in the transition from 3 to 5 nm is quite dramatic. While the 3 nm thick monolayer is mostly amorphous and filled with defects, the 5 nm film, consisting of two multilayers, predominantly exhibits a terraced morphology consisting of distinct circular grains arranged in islands and exhibits no pits. The width of the terraces typically range from 20-50 nm, and the grains vary in diameter from 100-300 nm. In locations where two or more terraced columns of grains intersect, circular 20-30 nm diameter 'holes' appear, similar to grain boundary triple points seen in inorganic thin film growth. Unlike organic films containing screw dislocations, here the terraces in each layer are separated individually into islands and have a closed circumference. It is interesting to compare the values of r.m.s roughness and step heights across the grain boundaries in these two films. The rms roughness in the 2 μm ×2 μm scan area is 2.62 nm, almost comparable to the film thickness. It falls to 1.5 nm for the 5 nm thick film. The step heights of the terraces in the 5 nm film are typically < 0.5 nm and are often found in multiples of 0.29 nm (inset line profile in Fig. 2D), one-half the DFH-4T unit cell *b* axis (Fig. 1C). This implies that the molecular long axes is aligned parallel to the substrate surface. The most important observation emerging from analysis of these STM images is that as the film thickness evolves from a single monolayer to two multilayers, the growth mode transitions from an amorphous to a two-dimensional layered motif. This is accompanied by a corresponding reduction in surface roughness and an orientation of the DFH-4T molecules laying flat on the first monolayer in contact with the Au surface as shown in Fig. 1C.

To understand how the DFH-4T film growth continues to evolve as the film transitions into the bulk, we studied two more films of thicknesses 9 and 12 nm, consisting of three and four monolayers respectively (Figures 3A,B). These organic films too exhibit a terraced grain growth and an absence of pits. The grain size distribution is comparable to that of the 5 nm film (150-350 nm diameter). Despite these similarities, there are differences in the growth. For example, regions of the 9 nm film clearly exhibit a clustering of grains, which appear as curved ridges growing over the flat terraces, not seen in the 5 nm film, where the grains cover the Au(111) surface uniformly in terraces. The clustering increases the rms roughness to 1.86 nm. Figures 3C,D show STM images of the 12 nm thick DFH-4T film in comparable scan ranges. Morphological similarities to the 5 nm and 9 nm films showing overlapping terraced grain growth are evident. However the curved ridges growing over the terraces become more pronounced, increasing the r.m.s roughness further to 2.57 nm. Most importantly, line profiles (Fig. 3D, inset) across the 12 nm film ridges reveal that the step heights are now much larger than in the 5 nm films and are multiples of ~ 2.9 nm. This is one-half the DFH-4T unit cell long axis dimension (*a* axis; Fig. 1B) and corresponds to the XRD-observed interlayer *d* spacing. The measured height between the arrows marked in the inset is 5.99 nm, one DFH-4T *a* axis unit cell dimension. Similar features are also observed for bulk DFH-4T film grown on SiO_2 showing that the grain growth pattern is likely to be general for DFH-4T.

It is interesting to analyze evolution in the rms roughness as a function of the film thickness. The roughest films are the 3 nm thick monolayers, comprising numerous pits, while the smoothest films are the 5 nm thick films, having a uniform surface with similarly shaped circular and well-connected grains. As film thickness increases to 9 and 12 nm, surface roughness increases, although not to the extent of the 3 nm monolayers. The origin of this increased roughness is mainly from grain clusters at the curved ridges, since the remainder of the film surface is relatively smooth with an r.m.s roughness ~ 1 nm.

The STM results and the analysis presented above provides an understanding of the similarities and differences in growth of DFH-4T and other organic semiconductors. Interestingly terraced layered growth is also observed in the growth of various other organic films on many different substrates as well as in inorganic oxides and semiconducting films on various lattice-matched substrates. This similarity in the growth pattern for diverse organic films suggests that terraced grain growth is a common mode for organic semiconductors, independent of the substrate. This suggests that beyond the first few monolayers, molecular structure and stereochemistry play a greater role in shaping the dynamics of organic film growth than do orientation and lattice matching with the substrate.

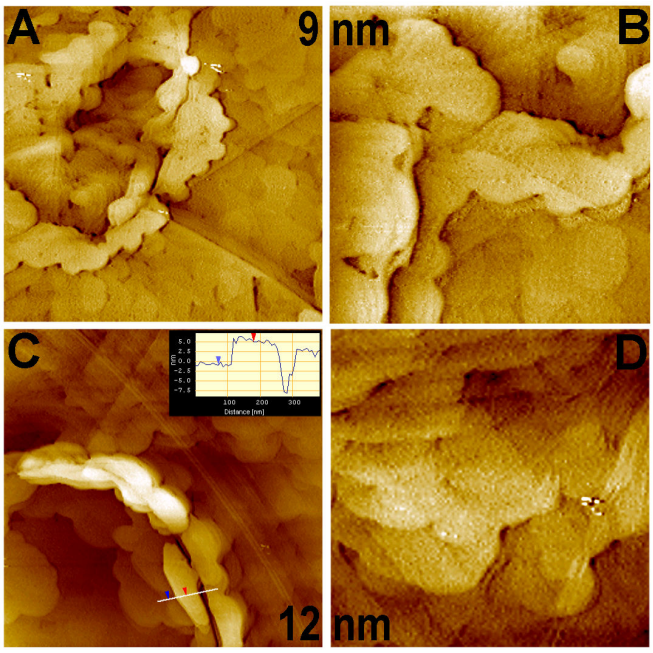

Fig. 3 Morphology of 9 nm and 12 nm thick films in 2 μm (right) and 1 μm (left) scans. Inset shows a profile cross a ridge with a step height of 5.99 nm.

To obtain information about the band gap of the DFH-4T monolayers, scanning tunneling spectroscopy (STS) was performed on the films. Figure 4A shows the differential conductance, dI/dV, proportional to the molecular density of states (DOS), which shows a gap of ~ 2.2 eV where the conductivity is very low. This STS-derived DOS value of for DFH-4T/Au(111) is slightly lower than the DOS obtained for DFH-4T from optical and electrochemical studies in solution (~2.8-2.9 eV). This could be due to strong interactions between the oligomer and the gold contacts leading to broadening of the energy levels in the monolayer.

The electronic transport of OFETs is presented in Figure.4B. Mobilities (μ) were calculated from the transfer plots in the saturation regime from: $\mu_{sat} = (2I_{DS}L)/[WC_{ox}(V_G-V_{th})^2]$ where I_{DS} is the source-drain saturation current; W (0.5-5.0 mm) and L (25-300 μm) are the channel width and length, respectively; C_{ox} (10 nF/cm^2) is the oxide capacitance, V_G is the gate voltage, and V_{th} is the threshold voltage. Parallel electrical characterization of top- vs. bottom-contact configuration DFH-4T FETs with Au source/drain electrodes reveals greatly different mobilities (μ_{TOP} = 1.1±0.2 10^{-2} cm^{2}V^{-1}s^{-1} vs. μ_{BOTTOM} = 2.3±0.5 10^{-5} cm^{2}V^{-1}s^{-1}) and contact resistances ($R_{C\text{-}TOP}$ = 4-12 MΩcm vs. $R_{C\text{-}BOTTOM}$ > 1 GΩcm). The other OFET parameters are: $(I_{on}:I_{off})_{TOP}$ = 4±2 10^7; $(I_{on}:I_{off})_{BOTTOM}$ = 7±25 10^3; $(V_T)_{TOP}$ = 64±7 V; $(V_T)_{BOTTOM}$ = 66±11 V; $(V_{on})_{TOP}$ = 20 V; $(V_{on})_{BOTTOM}$ = 20-30 V. All this data underscores the superior performance metrics of top-contact devices. Note that the difference between V_T (~ 65V) and V_{on} (~ 20 V) for optimum samples is identical for both

top and bottom device structures (ΔV ~ 45 V), suggesting similar dielectric-semiconductor interfacial trap densities. Therefore, the current output variations must reflect different electron injection efficiencies from the Au contacts and not arise from variations in DFH-4T film quality or its interface with the dielectric. These observations raise intriguing questions about the origin of such large bottom-contact resistances, the large differences in top- vs. bottom-contact resistance and therefore, the OFET performance differences ($\Delta R > 10^3$ Ωcm, $\Delta\mu > 10^3$ $cm^2V^{-1}s^{-1}$) for fluorinated organic semiconductors. This is particularly intriguing since OFETs from other small molecules such as pentacene behave very differently (ΔR ~ 0-20 Ωcm, $\Delta\mu$ ~ 0-5 $cm^2V^{-1}s^{-1}$) [4], with much smaller performance differences between the top and bottom contact devices.

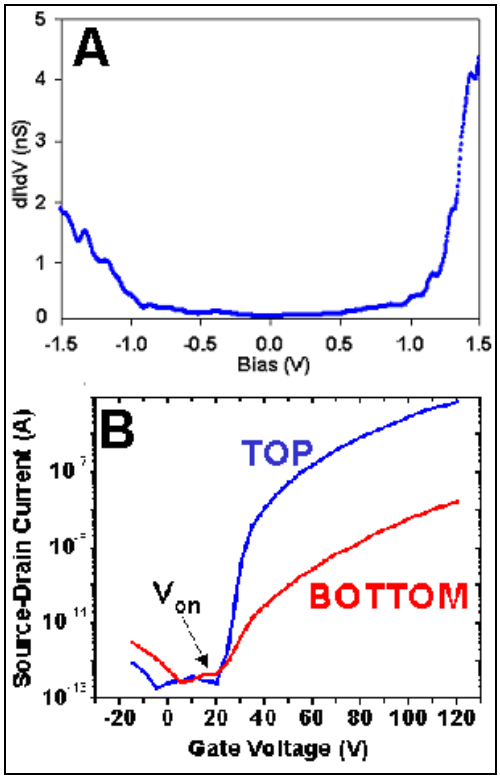

Fig. 4 (a) Tunneling I-V of DFH-4T film showing a band gap of 2.25 eV. (b) Transfer plots for top and bottom contact OFETs with V_{SD} 100V.

The OFET results can be understood by an analysis of the morphological evolution of the DFH-4T organic layer as a function of thickness and an analysis of the step height variations revealed in the STM study. These highlight many important aspects of DFH-4T film growth and also explain the large DFH-4T bottom-contact resistances observed in the OFET devices. The first monolayer on Au(111) is disordered, amorphous and has a larger number of pits and defects which could act as electron traps. In contrast, thicker films exhibit a remarkable nanostructural evolution with the formation of well-defined crystallites, terraces, and grain boundaries. The step heights of films having fewer monolayers (e.g., the 5 nm film) indicate that the molecules lie *parallel* to the Au surface. As the film thickness increases to greater than two monolayers, larger number of molecules now pack in the crystalline layers with step height in multiples of ~ 2.9 nm, ie. with the long axes aligned *perpendicular* to the Au surface. Thus, three major nanostructure and molecular orientation changes occur before DFH-4T film growth on Au transitions to the bulk. The high DFH-4T monolayer interfacial roughness and poor molecular alignment are the principal origins of the large bottom-contact resistance on the OFETs. The contact resistance for top-contact OFET devices are much smaller and this can be understood from an absence in the thicker DFH-4T films of disruptive growth morphologies within the semiconducting channel and the presence of large, smooth crystallite terraces on which Au should deposit uniformly, thereby not compromising device performance. Perpendicular orientation of the of the molecules further results in better overlap of the molecular cores and in efficient charge transport.

Conclusion

We have presented the evolution in the growth morphology of N-type fluoro functionalized oligothiophene DFH-4T on Au(111) during a transition from one monolayer to many multilayers and concurrent top and bottom contact device characteristics. This study elucidates the nature of the interface between the organic semiconductor and source-drain electrodes in OFET devices. The pitted and disordered monolayer results in poor mobilities for bottom contact OFETs. Reorientation of the molecules in multilayers by 90° results in efficient stacking and overlap of pi orbitals with an associated increase in top contact OFET mobility by three orders of magnitude. The results provide direct and generalizable information as to why DFH-4T bottom contact devices perform less optimally as compared to their top-contact counterparts.

References:

[1] Street, R. A.; Wong, W. S.; Ready, S. E.; Chabinyc, M. L.; Arias, A. C.; Limb, S.; Salleo, A.; Lujan, R. *Materials Today* **2006**, *9*, 32.
[2] G. R. Dholakia, A. Facchetti and T. J. Marks, Nano Lett. **6**, 2447 (2006).
[3] Facchetti, A.; Mushrush, M.; Katz, H. E.; Marks, T. J. *Adv. Mater.* **2003**, 15, 33.
[4] Burgi, L.; Richards, T. J.; Friend, R. H.; Sirringhaus, H. *J. Appl. Phys.* **2003**, *94*, 6129.

a) gdholakia@mail.arc.nasa.gov
b) a-facchetti@northwestern.edu
c) t-marks@northwestern.edu